

Monte Carlo model of electron energy degradation in a CO₂ atmosphere

Anil Bhardwaj and Sonal Kumar Jain

Space Physics Laboratory, Vikram Sarabhai Space Centre, Trivandrum
695022, India

Published in Journal of Geophysical Research, Vol. *114*, A11309 (2009),
doi:10.1029/2009JA014298

arXiv:1011.4398v1 [astro-ph.EP] 19 Nov 2010

—

Abstract. A Monte Carlo model has been developed to study the degradation of ≤ 1000 eV electrons in an atmosphere of CO_2 , which is one of the most abundant species in Mars' and Venus' atmospheres. The e- CO_2 cross sections are presented in an assembled set along with their analytical representations. Monte Carlo simulations are carried out at several energies to calculate the "yield spectra", which embodied all the information related to electron degradation process and can be used to calculate "yield" (or population) for any inelastic process. The numerical yield spectra have been fitted analytically resulting in an analytical yield spectra (AYS). We have calculated the mean energy per ion pair and efficiencies for various inelastic processes, including the double and dissociative double ionization of CO_2 and negative ion formation. The energy distribution of the secondary electrons produced per incident electron is also presented at few incident energies. The mean energy per ion pair for CO_2 is 37.5 (35.8) eV at 200 (1000) eV, compared to experimental value 32.7 eV at high energies. Ionization is the dominant loss process at energies above 50 eV with contribution of $\sim 50\%$. Among the excitation processes, 13.6 eV and 12.4 eV states are the dominant loss processes consuming $\sim 28\%$ energy above 200 eV. Around and below ionization threshold, 13.6 eV, 12.4 eV, and 11.1 eV, followed by 8.6 eV and 9.3 eV excitation states are important loss processes, while below 10 eV vibrational excitation dominates.

1. Introduction

Photoionization is the main source of electrons and ions in the dayside upper atmosphere of planets. Photoelectrons, generated due to photoionization process, can have enough kinetic energy to ionize the atmospheric constituents and produce secondary electrons. Similarly, energetic electrons precipitating along the magnetic field lines into the auroral atmosphere of planets can ionize the medium producing secondary electrons. Besides ionization, the electron energy is lost in excitation, attachment, and dissociation. Hence, the study of electron energy deposition in atmosphere is an important aspect in understanding processes like aurora, dayglow, nightglow [e.g., *Bhardwaj and Gladstone*, 2000; *Fox et al.*, 2008]. To model the electron energy degradation in an atmosphere one has to first compile cross sections for various loss processes, and then develop an electron energy apportionment method, which will distribute the electron energy among different loss channels.

The study of the electron energy degradation in CO₂ is of fundamental interest in various fields of science. CO₂ is one of the most important molecules in our solar system. It comprises more than 90% of the atmospheres of Venus and Mars. It is also used in lasers, gaseous discharge or low power plasma device. Electron energy degradation in CO₂ gas has important applications to Mars and Venus. Earlier results from Mariner satellites and Mars 3 and Mars 4 spacecrafts have confirmed the presence of an ionosphere on Mars, and also detected various emission features on Mars [e.g., *Barth et al.*, 1971; *Dementyeva et al.*, 1972], which have been studied in detail by recent SPICAM ultraviolet spectrometer observations aboard Mars Express [e.g., *Bertaux et al.*, 2006; *Leblanc et al.*, 2006]. Emissions from Venus have been studied quite extensively by Pioneer Venus [e.g., *Fox and Bougher*, 1991] and by the ongoing Venus Express [e.g., *Bertaux et al.*, 2007]. Electron impact excitation and dissociative excitation of CO₂ are the key processes in the production of several emissions on Mars and Venus.

In this paper we present a Monte Carlo model which describes the energy degradation of ≤ 1000 eV electrons in an atmosphere of CO₂. Earlier studies of electron degradation in CO₂ have been carried out by *Sawada et al.* [1972], *Green et al.* [1977], and *Fox and Dalgarno* [1979]. Monte Carlo methods are class of numerical methods based on stochastic technique. Though it is time consuming, but due to its probabilistic nature, it is an excellent technique for studying the energy degradation of particles, provided sufficient sample size is taken. Hence, Monte Carlo methods have been widely used in problems dealing with energetic particle degradation in gases and in applications to the planetary atmospheres [e.g., *Cicerone and Bowhill*, 1971; *Ashihara*, 1978; *Green et al.*, 1977, 1985; *Singhal et al.*, 1980; *Singhal and Green*, 1981; *Singhal and Bhardwaj*, 1991; *Bhardwaj and Singhal*, 1993; *Michael and Bhardwaj*, 2000; *Bhardwaj and Michael*, 1999a, b; *Shematovich et al.*, 2008].

In section 2, we present a compilation of all the e-CO₂ loss processes cross sections available up to the present date and fitted them with a simple analytical form. These analytically fitted cross sections can be easily used in the Monte Carlo model, which is presented in section 3. The output of the Monte Carlo simulation is employed to generate a “yield spectrum,” which is presented in section 4. The concept of the yield spectrum was first introduced by *Green et al.* [1977] and further developed by many workers [e.g., *Green and Singhal*, 1979; *Singhal and Green*, 1981; *Singhal and Haider*, 1984; *Green et al.*, 1985;

Singhal and Bhardwaj, 1991; Bhardwaj and Singhal, 1993; Bhardwaj and Michael, 1999a]. The yield spectra embodied the information about the electron degradation processes and can be used to calculate “yield” for any inelastic event. The numerical yield spectrum is represented in an analytical form resulting in an analytical yield spectrum (AYS). The AYS and its comparison with the numerical yield spectrum is also presented in the section 4. In sections 5 and 7, we present the calculated mean energy per ion pair and efficiencies for inelastic processes, respectively, using AYS and compare them with that obtained by using numerical yield spectra. The energy distribution of secondary and tertiary electrons produced during ionization events is presented in section 6. Summary of the paper is presented in section 8.

2. Cross sections

2.1. Total

The laboratory measured total scattering cross section (TCS) is available between 0.1 eV and 5000 eV. The TCS for e-CO₂ collision has been measured by several authors in different energy ranges – *Ferch et al. [1981]* in the energy range 0.007-4.5 eV, *Buckman et al. [1987]* 0.1-5 eV, *Szmytkowski et al. [1987]* 0.5-3000 eV, *Kimura et al. [1997]* 0.8-500 eV, *Kwan et al. [1983]* 1-500 eV, and *Garcia and Manero [1996]* 400-5000 eV. At low energies, the TCS of *Szmytkowski et al. [1987]*, *Buckman et al. [1987]*, and *Ferch et al. [1981]* are in agreement to within 10%. Recently, *Zecca et al. [2002]* have determined the best value of TCS. In the lowest energy range (<1 eV) *Zecca et al. [2002]* adopted the experimental data of *Ferch et al. [1981]* and *Buckman et al. [1987]*, which are in good agreement with each other. In the 1-1000 eV energy range, *Zecca et al. [2002]* averaged the cross sections obtained by *Szmytkowski et al. [1987]*, *Kimura et al., [1997]* and *Kwan et al. [1983]*, with equal weight, to obtain the recommended values, which are in good agreement with *Garcia and Manero [1996]* at higher (>400 eV) energies. In his review, *Itikawa [2002]* has recommended the TCS of *Zecca et al. [2002]*. The TCS reaches a maximum value of $60 \times 10^{-16} \text{ cm}^2$ at 0.1 eV [*Ferch et al., 1981; Buckman et al., 1987*], it then goes through a minimum of $5.5 \times 10^{-16} \text{ cm}^2$ at 1.9 eV [*Szmytkowski et al. 1987*]. At lower energies a resonant structure is present ~ 3.8 eV.

2.2. Elastic

2.2.1. Differential elastic

The differential elastic scattering cross section (DCS) for e-CO₂ collision has been measured by many authors [cf. review by *Itikawa, 2002; Karwasz et al., 2001*].

In the 1-4 eV energy, the DCS values of *Gibson et al. [1999]* and *Tanaka et al. [1998]* are in good agreement at forward angles ($\leq 50^\circ$), however at larger angles they differ by 20-30%. Overall, at most of the energies there are good agreement in shape between these two DCS. At 30, 40, and 50 eV, the DCS measurements of *Gibson et al. [1999]*, *Kanik et al. [1989]*, and *Tanaka et al. [1998]* are in reasonable accord, within the uncertainties of each measurement, and at 50 eV the DCS of *Gibson et al. [1999]* and *Register et al. [1980]* are consistent. At 100 eV, the measured DCS values of *Iga et al. [1999]* are in good agreement with *Kanik et al. [1989]* and *Tanaka et al. [1998]*.

We have taken the DCS values from *Tanaka et al. [1998]* in the 1-100 eV range, however values at 40, 50, 70, 80, and 90 eV are taken from *Kanik et al. [1989]* which agree well with the cross section of *Tanaka et al. [1998]* in the entire energy range. The DCS values

in 200-400 eV range are taken from *Iga et al.* [1999], and those in 500-1000 eV are taken from *Iga et al.* [1984]. In Table 1, we present the DCS values used in this work.

2.2.2. Total elastic

Based on the DCS measured by *Register et al.* [1980], *Tanaka et al.* [1998] and *Gibson et al.* [1999], *Buckman et al.* [2002] have determined the total elastic cross section in 1-100 eV range with an estimated uncertainty of $\pm 30\%$. *Shirai et al.* [2001] have reported the recommended elastic cross section up to 1000 eV by considering the beam data of *Iga et al.* [1999]. *Itikawa* [2002] has recommended the elastic cross section of *Buckman et al.* [2002] in the energy range 1-60 eV, and *Shirai et al.* [2001] in the energy range 100-1000 eV. The two data sets merge smoothly .

We have taken total elastic cross section as recommended by *Itikawa* [2002]. The total elastic cross section is fitted using the semi-empirical formula [*Bhardwaj and Michael*, 1999a]:

$$\sigma(E) = \frac{1}{A_1 + B_1 E} + \frac{1}{A_2 + B_2 E} + \frac{2}{E} \frac{\sqrt{A_1 A_2}}{A_2 B_1 - A_1 B_2} \ln \frac{(1 + B_1 E/A_1)}{(1 + B_2 E/A_2)}, \quad (1)$$

where A_1, B_1, A_2 , and B_2 are the fitting parameters, whose values are $8.090 \times 10^{-16} \text{ \AA}^{-2}$, $2.184 \times 10^{-2} \text{ \AA}^{-2} \text{ keV}$, 0.92 \AA^{-2} and $5.0 \times 10^{-4} \text{ \AA}^{-2} \text{ keV}$, respectively, and E is the energy of the electron in eV. Lower limit of fit is 30 eV, and fitted cross section is shown in Figure 1. At energies below 30 eV it is difficult to fit the cross section using above equation due to resonance structure present at low energies (~ 4 eV), and hence these values are fed numerically in the Monte Carlo model.

2.3. Dissociative electron attachment

The dissociative attachment process in e-CO₂ collisions, which mainly occurs at energies < 12 eV, leads to the formation of negative ions O⁻, O₂⁻, and C⁻. *Rapp and Briglia* [1965] measured absolute values of the total cross section for the production of negative ions from CO₂. *Orient and Srivastava* [1983] obtained the cross section for the production of O⁻ ions and showed that it is the dominant anion. Their values are in agreement with those of *Rapp and Briglia* [1965] within the uncertainty of the cross sections ($\pm 20\%$) and the energy scale (± 0.1 eV). *Spence and Schulz* [1974] measured the cross sections for the production of C⁻ and O₂⁻ ions. The cross section for O₂⁻ production has two peaks of the order of 10^{-24} cm^2 at 11.3 and 12.9 eV, while cross section for C⁻ production has three peaks with the largest value of $\sim 2 \times 10^{-21} \text{ cm}^2$. The cross sections for O₂⁻ and C⁻ are small compared to that of O⁻, and hence are not considered in our study.

We have adopted the cross section values of *Rapp and Briglia* [1965] for the production of O⁻ ions from CO₂. The cross section shows a double-peak structure – peaks at 4.1 and 8.3 eV, with the later peak value ($4.28 \times 10^{-19} \text{ cm}^2$) about 2.5 times the value of the former peak. The cross section for each peak has been fitted with the following analytical form [*Bhardwaj and Michael*, 1999a]:

$$\sigma(E) = \frac{Ae^t/U}{(1 + e^t)^2}, \quad (2)$$

Here $t = (E - W_p)/U$, where W_p is the energy at the peak. The values of the overall normalization parameter A and the effective width parameter U for each of the peaks

along with the parameter W_p and threshold energy W_{th} are presented in Table 2. The fitted cross sections along with laboratory measurements are given in Figure 2.

2.4. Ionization

The ionization and dissociative ionization of CO_2 by electron impact produce singly and doubly ionized ions (CO_2^+ , CO^+ , C^+ , O^+ , C^{++} , O^{++} , and CO_2^{++}). The cross sections for these processes have been reported by *Rapp and Englander-Golden* [1965], *Shyn and Sharp* [1979], *Orient and Srivastava* [1987], *Tian and Vidal* [1998], and *Straub et al.* [1996]. Recently, *McConkey et al.* [2008] have reviewed the electron impact dissociation cross sections for CO_2 . For the total ionization cross section, measurements of *Orient and Srivastava* [1987], *Tian and Vidal* [1998], and *Straub et al.* [1996] are within the error limits with values of *Rapp and Englander-Golden* [1965] upto 1000 eV, and with the data of *Shyn and Sharp* [1979] in the energy range 50-400 eV. *Tian and Vidal* [1998] have also measured the cross sections for double and triple ionization of CO_2 due to electron impact. After a survey of the available experimental data, *Lindsay and Mangan* [2002] suggested recommended values of ionization cross section. Their partial cross sections are based on measurement of *Straub et al.* [1996]. For total ionization cross section below 25 eV, *Lindsay and Mangan* [2002] adopted the values of *Rapp and Englander-Golden* [1965]. At energies above 25 eV, they reported uncertainties of 5% for the partial cross sections for the production of CO_2^+ , CO^+ , C^+ , O^+ , and the total ionization cross section. The cross sections at energies below 25 eV have uncertainties of 7%. There are also uncertainties in appearance energies of fragmented ions CO^+ , C^+ , O^+ , C^{++} , and O^{++} . We have taken the appearance energies for the fragmented ions from *Itikawa* [2002].

We have used the dissociative and direct ionization cross sections recommended by *Lindsay and Mangan* [2002] [cf. *Itikawa*, 2002; *McConkey et al.*, 2008]. The CO_2^+ ion can be produced in four excited states, viz., $X^2\Pi_g$, $A^2\Pi_u$, $B^2\Sigma_u^+$, and $C^2\Sigma_g^+$. Cross sections for $A^2\Pi_u$ and $B^2\Sigma_u^+$ states have been taken from *Itikawa* [2002], while the cross sections for $X^2\Pi_g$ and $C^2\Sigma_g^+$ states have been taken from *Jackman et al.* [1977]. For double ionization, cross sections of $(\text{CO}^+, \text{O}^+)$, (C^+, O^+) , and (O^+, O^+) production have been taken from *Tian and Vidal* [1998] up to 600 eV; these cross sections have not been added in the total ionization cross section because they are already accounted in the cross sections for the formation of CO^+ , C^+ , and O^+ ions. All these cross sections have been fitted using the analytical expression [*Jackman et al.*, 1977; *Bhardwaj and Michael*, 1999a].

$$\sigma(E) = A\Gamma \left[\arctan \frac{(T_M - T_0)}{\Gamma} + \arctan \left(\frac{T_0}{\Gamma} \right) \right], \quad (3)$$

where

$$A(E) = \left[\frac{K}{E + K_B} \right] \ln \left[\frac{E}{J} + J_B + \frac{J_C}{E} \right];$$

$$\Gamma(E) = \Gamma_S \left[\frac{E}{E + \Gamma_B} \right];$$

$$T_0(E) = T_S - \left[\frac{T_A}{E + T_B} \right]; \quad T_M = \frac{E - I}{2}.$$

Here E is the incident energy in eV, I is the fitting ionization potential in the eV, which is generally close to the threshold potential (W_{th}), and σ is in units of 10^{-16} cm^2 . This form

gives the asymptotic behavior $\sigma(E) \propto E^{-1} \ln E$ at high energies, which is expected from the Born approximation. The fitting parameters are presented in the Table 3. The fitted cross sections for single and double ionization are shown in Figures 3 and 4, respectively.

2.5. Excitation cross sections

2.5.1. Vibrational excitation

CO₂ is a linear triatomic molecule, which has three normal modes of vibration, *i.e.*, a bending mode (0 n 0), a symmetric stretching mode (n 0 0), and an asymmetric stretching mode (0 0 n), with excitation energy 83 meV, 172 meV, and 291 meV, respectively [Kochem *et al.*, 1985]. Infrared active (010) bending and (001) asymmetric stretching modes in the near-to-threshold region follow the Born approximation. Moreover, the structure near the threshold of vibration excitation in CO₂ has been investigated by Kochem *et al.* [1985], vibrationally inelastic DCS above 4 eV impact energies have been measured by Register *et al.* [1980] for scattering angles 10° – 140° and impact energies of 4, 10, 20, and 50 eV, and by Johnstone *et al.* [1995] for only one scattering angle (20°) in the energy region 1 to 7.5 eV. Nakamura [1995] determined the vibrational cross section using swarm experiment. Kitajima *et al.* [2001] made measurements of DCS for the electron impact excitation of CO₂ for (010), (100), (001), and (020) vibrational modes over the scattering angles 20° – 130° and energy range 1.5-30 eV (except at 4 eV where the smallest angle was extended upto 10°), and assigned an uncertainty of 30% to their measurements. Their DCS is consistent with the results of previous beam-type measurements. Itikawa [2002] has extrapolated the DCS of Kitajima *et al.* [2001] to obtain the total vibration cross sections for three modes, which are presented in Figure 1.

In our studies we have taken cross sections for the three fundamental vibrational modes (010), (100), and (001) from Itikawa [2002]. There are other modes also but their cross sections are small compare to these three fundamental modes.

2.5.2. Electronic excitation

There are several features in the optical and electron scattering spectrum of CO₂ in the energy loss range between 7 and 11 eV (Herzberg, 1966; Rabalais *et al.*, 1971; Hall *et al.*, 1973). Except for Rydberg states, there is still no definite consensus about structure and assignment of the excited electronic states of CO₂. In the energy loss spectra of CO₂, Green *et al.* [2002] have found four clearly distinct peaks at 10.98, 11.05, 11.16, and 11.40 eV, with an uncertainty of 30% in their results. Itikawa [2002] in his review paper has recommended the DCS of Green *et al.* [2002], for the excitation of the 10.8-11.5 eV energy loss states. Recently, Kawahara *et al.* [2008] have given the integral cross section for electronic states $^1\Sigma_u^+$ and $^1\Pi_u$ of CO₂, based on the DCS measurement of Green *et al.* [2002] in the energy range 20-200 eV.

Theoretical calculations of electronic structure have also been made by several authors [Nakatsuji, 1983; Spielfiedel *et al.*, 1992; Buenker *et al.*, 2000; Lee *et al.*, 1999]. Using distorted-wave method, Lee and McKoy [1983] calculated the cross section for the excitation of eight low lying-states. But there is not much agreement among these calculations. In summary, there is still a need for a detailed study of excitation of electronic states of CO₂ by electron impact.

We have taken the empirical cross sections of Jackman *et al.* [1977] for the electronic states of CO₂. These cross sections have been obtained using equation:

$$\sigma(E) = \frac{(q_0 F)}{W^2} \left[1 - \left(\frac{W}{E} \right)^\alpha \right]^\beta \left[\frac{W}{E} \right]^\Omega \quad (4)$$

where $q_0 = 4\pi a_0 R^2$ and has the value $6.512 \times 10^{-14} \text{ eV}^2 \text{ cm}^2$. The fitting parameters are given in Table 4. The parameters for the two states 12.4 and 13.6 eV, that corresponds to Cameron band of CO [cf. *Sawada et al.*, 1972] have been modified. The peak cross section of their sum is $2.40 \times 10^{-16} \text{ cm}^2$ at 80 eV [*Erdman and Zipf*, 1983].

2.6. Emission

Electron impact dissociation and ionization of CO_2 can result in the production of excited fragments of CO, O, and CO_2 in the neutral and ionized states, resulting in the emissions in the ultraviolet region. These emissions are important for understanding phenomena like aurora, dayglow that occur in the atmospheres of Mars, Venus, and CO_2 -containing atmospheres. The strong band systems observed on Mars are Fox-Duffendack-Barker bands ($A^2\Pi_u \rightarrow X^2\Pi_g$) and ultraviolet doublet ($B^2\Sigma_u^+ \rightarrow X^2\Pi_g$) of CO_2^+ , and Cameron bands ($a^3\Pi \rightarrow X^1\Sigma^+$) of CO [*Ajello*, 1971; *Barth et al.*, 1971; *Bertaux et al.*, 2006; *Leblanc et al.*, 2006]. *Ajello* [1971] measured the emission cross sections for the $A^2\Pi_u \rightarrow X^2\Pi_g$ and $B^2\Sigma_u^+ \rightarrow X^2\Pi_g$ bands of CO_2^+ from threshold to 300 eV. He also measured cross sections for the excitation of the fourth positive system of CO ($A^1\Pi \rightarrow X^1\Sigma^+$), the first negative system of CO^+ ($B^2\Sigma^+ \rightarrow X^2\Sigma^+$) and several atomic multiplets of carbon and oxygen produced from dissociative excitation of CO_2 .

2.6.1. Emission from CO_2^+

McConkey et al. [1968], *Ajello* [1971], and *Tsurubuchi and Iwai* [1974] have detected emissions corresponding to the following transitions:

$$A^2\Pi_u \rightarrow X^2\Pi_g \quad \text{at } 293.6 - 438.4 \text{ nm}$$

and

$$B^2\Sigma_u^+ \rightarrow X^2\Pi_g \quad \text{at } 218.9 - 226.8 \text{ nm}$$

The peak value of cross sections measured by the three groups for the above transitions are in good agreement with each other. These emissions are well known in the Mars upper atmosphere. Both the ground and excited states of CO_2^+ are known to be linear [*Herzberg*, 1966]. The cross section of *Ajello* [1971] has too steep an energy dependence near threshold compared to *McConkey et al.* [1968] and *Tsurubuchi and Iwai* [1974]. In his review, *Itikawa* [2002] recommended the cross sections of *Tsurubuchi and Iwai* [1974], for which the peak values are $(8.0 \pm 2.0) \times 10^{-17} \text{ cm}^2$ at 160 eV for the $A - X$ transition, and $(4.7 \pm 1.2) \times 10^{-17} \text{ cm}^2$ for the $B - X$ transition. We have taken the cross sections for $A - X$ and $B - X$ emissions of CO_2^+ from *Itikawa* [2002]. These cross sections have been fitted using equation (3). The fitting parameters are given in Table 3, and fitted cross sections in Figure 3.

2.6.2. Emission from CO^+

Only *Ajello* [1971] has measured the cross section for the emission of first negative system ($B^2\Sigma^+ \rightarrow X^2\Sigma^+$) of CO^+ . The cross section exhibits an appearance potential of 25.11 eV, and the peak value of cross section is $1.9 \times 10^{-18} \text{ cm}^2$ around 100 eV. The cross section for the excitation of the first negative system of CO^+ from electron impact on CO_2

is about a factor of 25 less than for excitation of the same system from CO [Ajello, 1971]. We have adopted the cross section of Ajello [1971], which has been fitted analytically using equation (4); the fitting parameters are given in Table 4. Figure 3 shows the fitted cross section along with experimental cross section.

2.6.3. Emission from CO

Cross sections for the production of Cameron band system ($a^3\Pi \rightarrow X^1\Sigma^+$) and fourth positive system ($A^1\Pi \rightarrow X^1\Sigma^+$) of CO have been measured by Ajello [1971]. The emission cross section for the fourth positive system is very weak and Ajello could not measure the cross section near threshold (13.48 eV). For the Cameron band system, Ajello [1971] reported relative magnitudes of the cross section for the (0, 1) band at 215.8 nm. The upper state ($a^3\Pi$) of Cameron emission is metastable and has a long radiative lifetime (~ 3 ms) [Giliyamse *et al.*, 2007], and kinetic energies of the CO($a^3\Pi$) fragments are in the range of 0–1.2 eV [Freund, 1971]. Erdman and Zipf [1983] measured the total cross section for CO ($a^3\Pi \rightarrow X^1\Sigma^+$) electronic transition. They estimated the absolute magnitude of total Cameron band emission cross section of 2.4×10^{-16} cm² at 80 eV. The Cameron band is the brightest emission feature in the UV dayglows of both Mars and Venus as well as an important emission in CO₂-containing atmospheres, *e.g.* comets.

2.6.4. Emission from O and C

Both Ajello [1971] and Mumma *et al.* [1972] have reported cross section for the emission of the O 130.4 nm triplet from electron impact on CO₂, but the measurements are not consistent with each other. There are many other atomic emissions produced in e-CO₂ collisions, but they have very small cross sections [cf. van der Burgt *et al.*, 1989]. Kanik *et al.* [1993] have reported the emission cross sections for O, O⁺, C, C⁺, CO, and CO⁺ in the wavelength region 40 - 125 nm. All the cross sections of Kanik *et al.* [1993] are less than 10^{-18} cm². We have adopted the O I and C I production cross sections of Jackman *et al.* [1977].

3. Monte Carlo Model

The transport of radiation is a natural stochastic process that is amenable to the Monte Carlo method due to its probabilistic nature. In the Monte Carlo simulation, modeling of an inherently stochastic system is carried out by artificial random sampling. In the present work we have developed a Monte Carlo model to simulate the local degradation of 1-1000 eV electrons in an atmosphere of CO₂ gas. The energy bin size is taken as 1 eV throughout the energy range. In the simulation we have considered elastic scattering between electrons and neutral CO₂ molecules, and various inelastic processes like ionization, excitation, attachment, dissociation, etc; the cross sections for these processes are described in section 2. Figure 5 illustrates how an individual electron is treated in the Monte Carlo simulation.

The initial energy E_0 of the electron is fixed at the beginning of the simulation and the direction of movement of the electron (θ , ϕ) is decided with the help of two random numbers R_1 and R_2 [random numbers are uniformly distributed in the range (0, 1)] as

$$\theta = \cos^{-1}(1 - 2R_1), \quad (5)$$

$$\phi = 2\pi R_2. \quad (6)$$

The distance to next collision is calculated from

$$S = -\log(1 - R_3)/n\sigma_T, \quad (7)$$

where R_3 is a random number, n is the number density of the neutral target species (taken as $1 \times 10^{10} \text{ cm}^{-3}$), and σ_T is the total (elastic + inelastic) electron impact collision cross section. After generating a new random number R_4 , the probability of elastic collision $P_{el} = \sigma_{el}/\sigma_T$ is calculated. if $P_{el} > R_4$, elastic collision takes place. if $P_{el} \leq R_4$, the inelastic event takes place, and in this case we further test for the type of inelastic event that has taken place with the help of another random number.

For elastic scattering the energy loss is calculated as

$$\Delta E = \frac{m^2 v^2}{m + M} - \frac{m^2 v V_1 \cos \delta}{m + M}, \quad (8)$$

$$V_1 = v \left[\frac{m \cos \delta}{m + M} + \frac{[M^2 + m^2(\cos \delta - 1)]^{1/2}}{m + M} \right].$$

Here δ is the scattering angle in the laboratory frame, v and m are the velocity and mass, respectively, of the electron, and M is the mass of the target particle. Differential elastic cross sections (discussed in section 2.2.1) are used to obtain the scattering angle δ . Differential cross sections are fed numerically in the Monte Carlo model at 28 unequally spaced energy points (1.5, 2, 3, 3.8, 4, 5, 6, 6.5, 7, 8, 9, 10, 15, 20, 30, 40, 50, 60, 70, 80, 90, 100, 200, 300, 400, 500, 800, and 1000 eV) and at 20 scattering angles (0° , 5° , 10° , 15° , 20° , 30° , 40° , 50° , 60° , 70° , 80° , 90° , 100° , 110° , 120° , 130° , 135° , 150° , 165° , and 180°). At intermediate energies and angular points the values are obtained through linear interpolation. The energy ΔE is subtracted from the energy of the test particle. After the collision, the deflection angle relative to the direction (θ, ϕ) is obtained as

$$\cos \theta'' = \cos \theta \cos \theta' - \sin \theta \sin \theta' \cos \phi',$$

$$\cos \phi'' = (\cos \theta \cos \phi \sin \theta' \sin \phi' - \sin \phi \sin \theta' \sin \phi' + \sin \theta \cos \phi \cos \theta') / \sin \theta'', \quad (9)$$

$$\sin \phi'' = (\cos \theta \cos \phi \sin \theta' \cos \phi' - \cos \phi \sin \theta' \sin \phi' + \sin \theta \sin \phi \cos \theta') / \sin \theta''.$$

Here θ' , ϕ' are the scattering angles.

In the case of an inelastic collision, the next step is to find whether the event is ionization or any of the other type of inelastic collision. If the collision is an ionization event, a secondary electron is produced. The energy of the secondary electron T is calculated with the help of a random number R as [Bhardwaj and Michael, 1999a]

$$T = \frac{\Gamma_S E_v}{E_v + \Gamma_B} [\tan(RK_1 + (R - 1)K_2)] + T_S - \left[\frac{T_A}{E_v + T_B} \right], \quad (10)$$

where

$$K_1 = \tan^{-1} \left\{ \left[\frac{(E_v - I)}{2} - T_S + \frac{T_A}{(E_v + T_B)} \right] / \frac{\Gamma_S E_v}{(E_v + \Gamma_B)} \right\},$$

$$K_2 = \tan^{-1} \left\{ \left[T_S - \frac{T_A}{(E_v + T_B)} \right] / \frac{\Gamma_S E_v}{(E_v + \Gamma_B)} \right\}.$$

Here E_v is the energy of the incident primary electron before the ionization event. Γ_S , Γ_A , T_A , T_B , and T_S are the fitting parameters, and I is the ionization threshold. The values of these parameters are given in Table 3. If the energy of secondary electron, produced in the ionization event, is more than the lowest cutoff energy (which is 1 eV in our simulation) then it is also tracked in a same manner as the primary electron (cf. Figure 5). The secondary electrons can also cause ionization, producing tertiary electrons, which are treated in a similar way as secondary electrons. In the Monte Carlo simulation we also follow tertiary and subsequent electrons. The number of secondary, tertiary, and subsequent electrons produced during the ionization events are stored in the appropriate energy bins. After the type of collision event has been decided, the appropriate energy is subtracted from the energy of the particle. All the collision events are recorded in the appropriate energy bins corresponding to the energy of the electron at the time of collision. The history (track view) of a particle with each interaction event is traced until the electron energy falls below an assigned cutoff value, which is 1 eV. The sample size in the present study is 10^6 particles for each simulation.

4. Yield Spectra

When all the sampled electrons have been degraded, we get a two dimensional yield spectrum, which is a function of the spectral energy E and incident primary electron energy E_0 , defined as [Green *et al.*, 1977]:

$$U(E, E_0) = \frac{N(E)}{\Delta E}, \quad (11)$$

where $N(E)$ is the number of inelastic collision events for which the spectral energy of the electron is between E and $E + \Delta E$, where ΔE is the energy bin width, which is 1 eV in our model. This yield spectrum is related to the degradation spectrum or equilibrium flux $f(E, E_0)$ of *Spencer and Fano* [1954] by the equation

$$U(E, E_0) = \sigma_T(E) f(E, E_0), \quad (12)$$

where σ_T is the total inelastic collision cross section.

The analytical yield spectrum $U(E, E_0)$ embodies the nonspatial information of the degradation process. It represents the equilibrium number of electrons per unit energy at an energy E resulting from the local energy degradation of an incident electron of energy E_0 , and can be used to calculate the yield J_j of any state j at energy E_0 with the help of following equation:

$$J_j(E_0) = \int_{W_{th}}^{E_0} U(E, E_0) P_j(E) dE \quad (13)$$

where $P_j(E) = \sigma_j(E)/\sigma_T(E)$ is the probability of occurrence of the j th process whose threshold potential is W_{th} . The yield for a particular process obtained by using the above

equation is used in the following sections to calculate the mean energy per ion pair and efficiencies for various loss processes. Except at very low energies, yield spectrum $U(E, E_0)$ and probability of excitation $P_j(E)$ both vary with E in a much simpler manner than do $f(E, E_0)$ and $\sigma_j(E)$.

For many application purposes yield spectrum obtained by equation (11) is represented in the following form:

$$U(E, E_0) = U_a(E, E_0) H(E_0 - E - E_m) + \delta(E_0 - E). \quad (14)$$

Here H is the Heavyside function, with E_m being the minimum threshold of the processes considered, and $\delta(E_0 - E)$ is the Dirac delta function which allows for the contribution of the source itself. In atmospheric and astrophysical applications it is convenient to represent $U_a(E, E_0)$ in an analytical form [Green *et al.*, 1977]:

$$U_a(E, E_0) = A_1 \xi_0^s + A_2 (\xi_0^{1-t} / \epsilon^{3/2+r}) \quad (15)$$

Here $\xi = E_0/1000$ and $\epsilon = E/I$ (I is equal to lowest ionization threshold). $A_1 = 0.027$, $A_2 = 1.20$, $t = 0$, $r = 0$, and $s = -0.0536$ are the best fit parameters.

We have also tried two other analytical forms given by *Singhal et al.* [1980] and *Green et al.* [1985]. The form given by *Singhal et al.* [1980] is:

$$U_a(E, E_0) = C_0 + C_1 \chi + C_2 \chi^2 \quad (16)$$

Here $\chi = E_0^\Omega / (E + L)$; where $\Omega = 0.585$ and $L = 1.0$ and E_0 is in keV, $C_0 = 0.0185$, $C_1 = 5.98$, and $C_2 = 210.4$ are fitted parameters. The analytical form given by *Green et al.* [1985] is:

$$U_a(E, E_0) = C_0 + C_1 (E_k + K) / [(E - M)^2 + L^2]. \quad (17)$$

Here $E_k = E_0/1000$, and C_0 , C_1 , K , M , and L are the fitted parameters which are independent of the energy. The values of these constant parameters are $C_0 = 0.0299$, $C_1 = 430$, $K = 0.0041$ keV, $M = 0.31$ eV, and $L = 1.9$ eV.

In obtaining our analytical fits we did not include values of the yield spectra very close to E_0 because in this regime yield spectra contain the rapid oscillations known as ‘‘Lewis effect’’ [cf. *Douthat*, 1975]. These oscillations are channels with a finite number of threshold energies, so that there are only certain energies near E_0 which an electron can acquire. Obviously, no electron can acquire an energy between E_0 and $E_0 - E_m$, and that is why the Heavyside function H is inserted in the first term on the right-hand side of equation (14). The numerical yield spectrum represented analytically using equations (15), (16), and (17) is the two-dimensional analytical yield spectrum (AYS). In our studies, we have used the AYS obtained using equation (15), which is presented in Figure 6 along with the numerical yield spectra obtained by using (14). It is clear from Figure 6 that the analytical spectra represents quite well the numerical yield spectra above the ionization threshold; however, at lower energies (below 15 eV) the AYS departs from the numerical yield spectra. Similar behavior is seen in the AYS of *Green et al.* [1977].

To overcome this deficiency we introduce an additional function to modify the lower energy part of the AYS:

$$U_b(E, E_0) = \frac{E_0 A_0 e^x / A_1}{(1 + e^x)^2}, \quad (18)$$

Here $x = (E - A_2)/A_1$, and A_0 , A_1 , and A_2 are the fitting parameters. The values of parameters are $A_0 = 10.095$, $A_1 = 5.5$, and $A_2 = 0.9$. Equation (18) only affects the lower energy (≤ 15 eV) part of the fit. The final AYS is the sum of equations (15) and (18) which is shown in Figure 6 at several incident energies: depicting a better fit at lower energies (> 5 eV) as well as at higher energies.

Because of the simplicity of function and cost effective computational advantage, the AYS technique has been widely used in different planetary atmospheres for various aeronomical calculations, like steady state electron fluxes and volume production rates for any ionization or excitation state; the details of the computational technique are described in earlier papers [e.g., *Singhal and Haider*, 1984; *Bhardwaj and Singhal*, 1993; *Singhal and Bhardwaj*, 1991; *Bhardwaj et al.*, 1990, 1996; *Bhardwaj*, 1999, 2003; *Bhardwaj and Michael*, 1999a, b; *Michael and Bhardwaj*, 2000; *Haider and Bhardwaj*, 2005].

5. Mean Energy per Ion Pair

The mean energy per ion pair, μ_j , is defined as the incident energy E_0 divided by the number of ion pairs produced. It can be expressed as

$$\mu_j(E_0) = E_0 / J_j(E_0), \quad (19)$$

where $J_j(E_0)$ is the population of the j th ionization process obtained by equation (13). The quantity mean energy per ion pair is known to approach a constant value at higher energies.

Figure 7 shows the mean energy per ion pair for the ions CO_2^+ (including the ground and excited states), CO^+ , O^+ , C^+ , CO_2^{++} , O^{++} and C^{++} along with the mean energy per ion pair for neutral CO_2 , solid symbol represents the mean energy per ion pair for neutral CO_2 obtained directly from the Monte Carlo simulation at few energy points.

Mean energy for all the ions decreases very rapidly above their threshold value, but after ~ 100 eV μ declines slowly and at higher energies it becomes almost constant. The values of μ for CO_2^+ , CO^+ , O^+ , and C^+ at 200 (1000) eV are 53.6 (51.2), 403 (415), 263.1 (247.8), and 626.7 eV (576.2) eV, respectively. The mean energy per ion pair for neutral CO_2 gas is 37.5 (35.8) eV at 200 (1000) eV. *Fox and Dalgarno* [1979] reported a value of 33.1 eV at 200 eV for the μ , while *Green et al.* [1977] obtained a value of 34.7 eV at 200 eV from their MDEB method. The measured value of the mean energy per ion pair in neutral CO_2 is 32.7 at high energies [*Klots*, 1968]. Mean energy per ion pair for $\text{X}^2\Pi_g$, $\text{A}^2\Pi_u$, $\text{B}^2\Sigma_u^+$, and $\text{C}^2\Sigma_g^+$ states of CO_2^+ at 200 (1000) eV are 112.3 (118.4), 180.3 (156), 301.5 (266.4), and 1999 (1222) eV, respectively.

6. Secondary Electron Distribution

During the degradation process, every time the electron undergoes an ionization collision event, a secondary electron is produced. The energy of the secondary electron produced

is calculated using (10). The maximum energy of the secondary electron produced can be $(E - I)/2$, where E is the energy of the colliding electron and I is the ionization potential. As mentioned before, secondary and tertiary electrons are also treated in the same manner as the primary electrons in the Monte Carlo model. The energy distribution of secondary electrons is presented in Figure 8 at several incident energies showing the number of secondary electrons produced per incident primary electron. The energy distributions of tertiary and quaternary electrons, which are presented only at $E_0 = 1000$ eV, are much steeper than that of secondary electrons. Each incident electron of $E_0 = 1000$ eV, at some point of its energy degradation process, produces at least one secondary or tertiary or quaternary electron, whose energy is <7 eV.

7. Efficiency

As the electron collide with the atmospheric particles, they lose their energy and finally become thermalized. The energy of the colliding electron is divided among the various inelastic loss processes. Efficiency means the fraction of incident energy of the electron which is eventually deposited in a particular loss channel after the completion of the entire degradation process. The efficiency, $\eta_j(E_0)$, of the j th process at incident energy E_0 can be obtained as

$$\eta_j(E_0) = \frac{W_{th}}{E_0} J_j(E_0) \quad (20)$$

We have calculated the efficiencies for all inelastic collisions using numerical yield spectra obtained from equation (14) and the AYS [sum of equations (15) and (18)].

Figure 9 presents efficiencies of various single ionization events producing CO_2^+ , CO^+ , O^+ , and C^+ . The CO_2^+ has the maximum efficiency throughout the energy region due its higher ionization cross section. At 1000 eV, $\sim 31\%$ energy of the incident electron goes into CO_2^+ formation, while 5.9%, 9.8%, and 5.0% energy goes into the production of CO^+ , O^+ , and C^+ , respectively. At higher energies (>100 eV), increase in the efficiencies for all ions is small, but near threshold it falls very rapidly. At threshold, efficiencies for CO_2^+ , CO^+ , O^+ , and C^+ are 5.1%, 1.1%, 0.16% and 0.19%, respectively, while at 200 eV these are 29%, 6.0%, 9.2%, and 4.6%, respectively. Efficiencies for $\text{CO}_2^+(\text{A-X})$, $\text{CO}_2^+(\text{B-X})$, and first negative band of $\text{CO}^+(\text{B-X})$ are also shown in Figure 9. At 200 (1000) eV, 12.2 (11.6)% of incident electron energy goes in to the emission $\text{CO}_2^+(\text{A-X})$, while 9.8 (11.4)% and 3.0 (3.3)% goes in to the emissions $\text{CO}_2^+(\text{B-X})$ and $\text{CO}^+(\text{B-X})$, respectively.

Figure 10 shows the efficiencies for double ionization of CO_2 . At 200 (1000) eV, efficiencies for CO_2^{++} , O^{++} , and C^{++} are 0.56 (0.67)%, 0.052 (0.12)%, and 0.092 (0.14)%, respectively. We have also calculated the efficiencies for $(\text{CO}^+, \text{O}^+)$, (C^+, O^+) , and (O^+, O^+) , based on cross sections of *Tian and Vidal* [1998], whose values are 2.7 (3.1)%, 1.8 (2.4)%, and 0.96 (1.1)% at 200 (1000) eV. It is clear from Figures 9 and 10, that efficiencies calculated from the model and those obtained by using AYS are in good agreement.

Efficiencies for various excitation processes are presented in Figure 11. The 13.6, 12.4, and 11.1 eV states dominate the excitation events having efficiencies 16 (15)%, 12 (13)%, and 4.7 (4.2)% at 200 (1000) eV, respectively. Efficiencies of various line emissions of atomic oxygen and carbon are shown in Figure 12. Efficiencies for O I (1304), O I (1356), C I (1279), C I (1329), C I (1561), and C I (1657), are 0.12 (0.13)%, 0.27 (0.28)%, 0.084

(0.089)%, 0.035 (0.030)%, 0.10 (0.093)%, and 0.19 (0.18)%, respectively, at 200 (1000) eV. Overall efficiencies calculated from numerical yield spectra and AYS for various emission and excitation events are in good agreement.

In Figure 13, we present a summary picture of the electron energy distribution in CO₂ for all the loss processes grouped into important loss channels. At higher (>50 eV) energies ionization is the dominant loss process with energy consumption of ~50%. At lower energies (<15 eV), 11.1, 12.4, 8.6, and 9.3 eV loss channels are more important. At energies below 10 eV, vibration becomes the main loss channel. We have also shown the efficiency for total attachment process, which produces negative ion O⁻. The efficiency for anion O⁻ production peaks around 8 eV with a value of 0.8%, while it is 0.15 (0.13)% at 200 (1000) eV. The total efficiency for double ionization, which results in the production of CO₂⁺⁺, O⁺⁺, and C⁺⁺ ions, is also depicted in the figure. The double ionization efficiency raises sharply above 40 eV, having value of 0.4 (0.7)% at 100 (200) eV. Around 1000 eV, double ionization efficiency is 0.9%, which is higher than that of 8.6 and 9.3 eV excitation states. On the other hand, at energies >100 eV efficiency for dissociative ionization is higher than that of the 13.6 and 12.4 eV states.

8. Summary

In this paper we have presented a Monte Carlo model for ≤ 1000 eV electron degradation in CO₂ gas. All the e-CO₂ collision cross sections are compiled and fitted analytically. The analytical cross sections are presented in figures along with the laboratory measured cross sections for direct comparison, and the fitting parameters are provided in tables. The output of the Monte Carlo model is used to calculate the numerical “yield spectra”, which is represented by an analytical form. This analytical yield spectra (AYS) can be used in planetary atmospheres to determine various aeronomical quantities. We have modified and improved the AYS presented by *Green et al.* [1977] and *Singhal et al.* [1980] by adding a term that provides a better analytical representation of yield spectra at lower (<15 eV) energies. The yield spectra is employed to compute the mean energy per ion pair and efficiency of various inelastic processes. The mean energy per ion pair for CO₂ is found to be 37.5 (35.8) at 200 (1000) eV. The energy distribution of secondary electrons produced per incident electron is presented at few incident energies.

Efficiency is an effective measure to know what fraction of the incoming particle energy goes into a particular loss channel. We have presented efficiencies for various inelastic events calculated by using the AYS as well as by using the numerical yield spectra obtained from the Monte Carlo model. Efficiencies obtained by the two methods are in good agreement. In addition to major inelastic processes, efficiencies are presented for the formation of negative ions, double and dissociative double ionization of CO₂, and total vibrational excitation in the (100), (010), and (001) states. Since the AYS do not represent well the numerical yield spectra at very low (<5 eV) energies, the yield for vibrational excitation and attachment processes calculated by the AYS would be approximate. Ionization is the dominant loss process at higher energies, above 100 eV ~50% energy goes into ionization. At energies around and below ionization threshold excitation processes become important, and at energy below 10 eV, vibration is the dominant loss channel consuming more than 70% energy. The 13.6 and 12.4 eV loss channels are also important, at 1000 eV, around 28% of incident particle energy goes in to these states. A part of these

states represents the emissions of Cameron band system, which is an important emission in atmospheres of Mars and Venus as well as on comets (*Bhardwaj and Raghuram*, 2009, in preparation).

Efficiencies presented in this paper can be applied to planetary atmospheres by folding them with electron production rate and integrating over the energy. These results will be useful in the modeling of aeronomical processes in atmospheres of Mars, Venus, and CO₂-containing atmospheres.

References

- Ajello, J. M. (1971), Emission cross sections of CO₂ by electron impact in the interval 1260-4500 Å, II, *J. Chem. Phys.*, *55*, 3169.
- Ashihara, O. (1978), Photoelectron fluxes in the cometary atmosphere, *Icarus*, *35*, 369.
- Barth, C. A., C. W. Hord, J. B. Pearce, K. K. Kelly, G. P. Anderson, and A. I. Stewart (1971), Mariner 6 and 7 ultraviolet spectrometer experiment: Upper atmosphere data, *J. Geophys. Res.*, *76*, 2213.
- Bertaux, J.-L., et al. (2006), SPICAM on Mars Express: Observing modes and overview of UV spectrometer data and scientific results, *J. Geophys. Res.*, *111*, 10S90.
- Bertaux, J.-L., et al. (2007), SPICAV on Venus Express: Three spectrometers to study the global structure and composition of the Venus atmosphere, *Planet. Space Sci.*, *55*, 1673.
- Bhardwaj, A. (1999), On the role of solar EUV, photoelectrons, and auroral electrons in the chemistry of C(¹D) and the production of CI 1931 Å in the cometary coma: A case for comet 1P/Halley, *J. Geophys. Res.*, *104*, 1929.
- Bhardwaj, A. (2003), On the solar EUV deposition in the inner comae of comets with large gas production rates, *Geophys. Res. Lett.*, *30*, PLA 2.
- Bhardwaj, A., and G. R. Gladstone (2000), Auroral emissions of the giant planets, *Rev. Geophys.*, *38*, 295.
- Bhardwaj, A., and M. Michael (1999a), Monte Carlo model for electron degradation in SO₂ gas: Cross sections, yield spectra, and efficiencies, *J. Geophys. Res.*, *104*, 24713.
- Bhardwaj, A., and M. Michael (1999b), On the excitation of Io's atmosphere by the photoelectrons: Application of the analytical yield spectral model of SO₂, *Geophys. Res. Lett.*, *26*, 393.
- Bhardwaj, A., and R. P. Singhal (1993), Optically thin H lyman alpha production on outer planets: Low-energy proton acceleration in parallel electric fields and neutral H atom precipitation from ring current, *J. Geophys. Res.*, *98*, 9473.
- Bhardwaj, A., S. A. Haider, and R. P. Singhal (1990), Auroral and photoelectron fluxes in cometary ionospheres, *Icarus*, *85*, 216.
- Bhardwaj, A., S. A. Haider, and R. P. Singhal (1996), Production and emission of atomic carbon and oxygen in the inner coma of comet Halley: Role of electron impact, *Icarus*, *120*, 412.
- Buckman, S. J., M. T. Elford, and D. S. Newman (1987), Electron scattering from vibrationally excited CO₂, *J. Phys. B*, *20*, 5175.

- Buckman, S. J., M. J. Brunger, and M. T. Elford (2002), in *Photon and Electron Interaction with Atoms, Molecules and Ions*, edited by Y. Itikawa, Landolt-Börnstein Vol.I/17, Subvolume D (Springer, Berlin).
- Buenker, R. J., M. Honigmann, H.-P. Liebermann, and M. Kimura (2000), Theoretical study of the electronic structure of carbon dioxide: Bending potential curves and generalized oscillator strengths, *J. Chem. Phys.*, *113*, 1046.
- Cicerone, R. J., and S. A. Bowhill (1971), Photoelectron fluxes in the ionosphere computed by a Monte Carlo method, *J. Geophys. Res.*, *76*, 8299.
- Douthat, D. A. (1975), Electron degradation spectra in helium, *Radiat. Res.*, *61*, 1.
- Dementyeva, N. N., V. G. Kurt, A. S. Smirnov, L. G. Titarchuk, and S. D. Chuvahin (1972), Preliminary results of measurements of UV emissions scattered in the Martian upper atmosphere, *Icarus*, *17*, 475.
- Erdman, P. W., and E. C. Zipf (1983), Electron-impact excitation of the Cameron system ($a^3\pi \rightarrow X^1\Sigma$) of CO, *Planet. Space Sci.*, *31*, 317.
- Ferch, J., C. Masche, and W. Raith (1981), Total cross section measurement for e-CO₂ scattering down to 0.07, *J. Phys. B*, *14*, L97.
- Fox, J. L., and A. Dalgarno (1979), Electron energy deposition in carbon dioxide, *Planet. Space Sci.* *27*, 491.
- Fox, J. L., and S. W. Bougher (1991), Structure, luminosity, and dynamics of the Venus thermosphere, *Space Sci. Rev.*, *55*, 357.
- Fox, J. L., M. I. Galand, and R. E. Johnson (2008), Energy Deposition in planetary atmospheres by charged particles and solar photons, *Space Sci. Rev.*, *139*, 3.
- Freund, R. S. (1971), Dissociation of CO₂ by electron impact with the formation of metastable CO($a^3\Pi$) and O(5S), *J. Chem. Phys.*, *55*, 3569.
- Garcia, G., and F. Manero (1996), Total cross sections for electron scattering by CO₂ molecules in the energy range 400-5000 eV, *Phys. Rev. A*, *53*, 250.
- Gibson, J. C., M. A. Green, K. W. Trantham, S. J. Buckman, P. J. O. Teubner, and M. J. Brunger (1999), Elastic electron scattering from CO₂, *J. Phys. B*, *32*, 213.
- Gilijamse, J. J., S. Hoekstra, S. A. Meek, M. Metsälä, S. Y. T. van de Meerakker, G. Meijer, and G. C. Groenenboom (2007), The radiative lifetime of metastable CO ($a^3\Pi$, $\nu=0$), *J. Chem. Phys.*, *127*, 221102.
- Green, A. E. S., and R. P. Singhal (1979), Microplume model of spatial yield spectra, *Geophys. Res. Lett.*, *6*, 625.
- Green, A. E. S., C. H. Jackman, and R. H. Garvey (1977), Electron impact on atmospheric gases, 2, Yield spectra, *J. Geophys. Res.*, *82*, 5104.
- Green, A. E. S., Dayashankar, P. F. Schippnick, D. E. Rio, and J. M. Schwartz (1985), Yield and concentration microplumes for electron impact on water, *Radiat. Res.*, *104*, 1.
- Green M. A., et al. (2002), Absolute differential cross sections for electron impact excitation of the 10.8-11.5 eV energy-loss states of CO₂, *J. Phys. B*, *35*, 567.
- Hall, R. I., A. Chutjian, S. Trajmar (1973), Electron impact excitation and assignment of the low-lying electronic states of CO₂, *J. Phys. B*, *6*, L264.
- Haider, S. A., and A. Bhardwaj (2005), Radial distribution of production rates, loss rates and densities corresponding to ion masses ≤ 40 amu in the inner coma of Comet Halley: Composition and chemistry, *Icarus*, *177*, 196-216.

- Herzberg, G. (1966), *Molecular Spectra and Molecular Structure, vol. III, Electronic Spectra and Electronic Structure of Polyatomic Molecules* (Van Nostrand Reinhold, New York).
- Iga, I., J. C. Nogueira, and M. -T. Lee (1984), Elastic scattering of electrons from CO₂ in the intermediate energy range, *J. Phys. B*, *17*, L185.
- Iga, I., M. G. P. Homem, K. T. Mazon, and M. -T. Lee (1999), Elastic and total cross sections for electron-carbon dioxide collisions in the intermediate energy range, *J. Phys. B*, *32*, 4373.
- Itikawa, Y. (2002), Cross sections for electron collisions with carbon dioxide, *J. Phys. Chem. Ref. Data*, *31*, 749.
- Jackman, C. H., R. H. Garvey, and A. E. S. Green (1977), Electron impact on atmospheric gases, I, Cross sections, *J. Geophys. Res.*, *82*, 5981.
- Johnstone, W. M., P. Akther, and W. R. Newell (1995), Resonant vibrational excitation of carbon dioxide, *J. Phys. B*, *28*, 743.
- Kanik, I., D. C. McCollum, and J. C. Nickel (1989), Absolute differential elastic scattering cross sections for electron impact on carbon dioxide in the intermediate energy region, *J. Phys. B*, *22*, 1225.
- Kanik, I., J. M. Ajello, and G. K. James (1993), Extreme ultraviolet emission spectrum of CO₂ induced by electron impact at 200 eV, *Chem. Phys. Lett.*, *211*, 523.
- Karwasz, G. P., S. Brusa, and A. Zecca (2001), One century of experiments on electron-atom and molecule scattering: a critical review of integral cross-sections. II. Polyatomic molecules, *Rivista del Nuovo Cimento*, *24*, 1
- Kawahara, H., H. Kato, M. Hoshino, H. Tanaka, L. Campbell, and M. J. Brunger (2008), Integral cross sections for electron impact excitation of Σ_u^+ and Π_u electronics states in CO₂, *J. Phys. B*, *41*, 85203.
- Kimura, M., O. Sueoka, A. Hamada, M. Takekawa, Y. Itikawa, H. Tanaka, and L. Boesten (1997), Remark on total and elastic cross sections for the electron and positron scattering from CO₂, *J. Chem. Phys.*, *107*, 6616.
- Kitajima, M., S. Watanabe, H. Tanaka, M. Takekawa, M. Kimura, and Y. Itikawa (2001), Differential cross sections for vibrational excitation of CO₂ by 1.5-30 eV electrons, *J. Phys. B*, *34*, 1929.
- Klots, C. E. (1968), Energy deposition mechanisms, in *Fundamental Processes in Radiation Chemistry*, edited by Peter Ausloos, chap. 1, p. 40, Inter-science, New York.
- Kochem, K. -H., W. Sohn, N. Hebel, K. Jung, and H. Ehrhardt (1985), Elastic electron scattering and vibrational excitation of CO₂ in the threshold energy region, *J. Phys. B*, *18*, 4455.
- Kwan, C. K., Y.-F. Hsieh, W. E. kauppila, S. J. Smith, T. S. Stein, M. N. Uddin, and M. S. Dababneh (1983), e[±]-CO and e[±]-CO₂ total cross-section measurements, *Phys. Rev. A*, *27*, 1328.
- Leblanc, F., O. Witasse, J. Winningham, D. Brain, J. Lilensten, P.-L. Blelly, R. A. Frahm, J. S. Halekas, and J.-L. Bertaux (2006), Origins of the Martian aurora observed by Spectroscopy for Investigation of Characteristics of the Atmosphere of Mars (SPICAM) on board Mars Express, *J. Geophys. Res.*, *111*, A09313.
- Lee, C.-H., C. Winstead, and V. McKoy (1999), Collisions of low-energy electrons with CO₂, *J. Chem. Phys.*, *111*, 5056.

- Lee, M.-T., and V. McKoy (1983), Cross sections for electron impact excitation of the low-lying electronic states of CO₂, *J. Phys. B.*, *16*, 657.
- Lindsay B. G., and M. A. Mangan (2002), in *Photon and Electron Interaction with Atoms, Molecules and Ions*, edited by Y. Itikawa, Landolt-Börnstein Vol.I/17, Subvolume C (Springer, Berlin).
- McConkey, J. W., D. J. Burns, and J. M. Woolsey (1968), Absolute cross sections for ionization and excitation of CO₂ by electron impact, *J. Phys. B*, *1*, 71.
- McConkey, J. W., C. P. Malone, P. V. Johnson, C. Winstead, V. McKoy, and I. Kanik (2008), Electron impact dissociation of oxygen-containing molecules-A critical review, *Physics Reports*, *466*, 1.
- Michael, M., and A. Bhardwaj (2000), FUV emissions on Io: Role of Galileo-observed field-aligned energetic electrons, *Geophys. Res. Lett.*, *27*, 3137.
- Mumma, M. J., E. J. Stone, W. L. Borst, and E. C. Zipf (1972), Dissociative excitation of vacuum ultraviolet emission features by electron impact on molecular gases. III. CO₂, *J. Chem. Phys.*, *57*, 68.
- Nakamura, Y. (1995), Drift velocity and longitudinal diffusion coefficient of electron in CO₂-Ar mixtures and electron collision cross sections for CO₂ molecules, *Aust. J. Phys.*, *48*, 357.
- Nakatsuji, H. (1983), Cluster expansion of the wavefunction, valence and rydberg excitations, ionizations, and inner-valence ionizations of CO₂ and N₂O studied by the sac and sac CI theories, *Chem. Phys.*, *75*, 425.
- Orient, O. J., and S. K. Srivastava (1983), Production of O⁻ from CO₂ by dissociative attachment, *Chem. Phys. Lett.*, *96*, 681.
- Orient, O. J., and S. K. Srivastava (1987), Electron impact ionisation of H₂O, CO, CO₂, and CH₄, *J. Phys. B*, *20*, 3923.
- Rabalais, J. W., J. M. McDonald, V. Scherr, and S. P. McGlynn (1971), Electronic spectroscopy of isoelectronic molecules. II. Linear triatomic grouping containing sixteen valence electron, *Chem. Rev.*, *71*, 73.
- Rapp, D., and D. D. Briglia (1965), Total cross sections for ionization and attachment in gases by electron impact: II. Negative ion formation, *J. Chem. Phys.*, *43*, 1480.
- Rapp, D., and P. Englander-Golden (1965), Total cross sections for ionization and attachment in gases by electron impact: I. Positive ionization, *J. Chem. Phys.*, *43*, 1464.
- Register, D. F., H. Nishimura, and S. Trajmar (1980), Elastic scattering and vibrational excitation of CO₂ by 4, 10, 20, and 50 eV electrons, *J. Phys. B*, *13*, 1651.
- Sawada, T., D. J. Strickland, and A. E. S. Green (1972), Electron energy deposition in CO₂, *J. Geophys. Res.*, *77*, 4812.
- Shematovich, V. I., D. V. Bisikalo, J.-C. Grard, C. Cox, S. W. Bougher, F. Leblanc (2008), Monte Carlo model of electron transport for the calculation of Mars dayglow emissions, *J. Geophys. Res.*, *113*, E02011.
- Shirai, T., T. Tabata, and H. Tawara (2001), Analytical cross sections for electron collisions with CO, CO₂, and H₂O, relevant to edge plasma impurities, *Atom. Data Nucl. Data Tables*, *79*, 143.
- Shyn, T. W., and W. E. Sharp (1979), Doubly differential cross section of secondary electrons ejected from gases by electron impact: 50-400 eV on CO₂, *Phys. Rev. A*, *20*, 2332.

- Singhal, R. P., and A. E. S. Green (1981), Spatial aspects of electron energy degradation in atomic oxygen, *J. Geophys. Res.*, *86*, 4776.
- Singhal, R. P., and S. A. Haider (1984), Analytical yield spectrum approach to photoelectron fluxes in the Earth's atmosphere, *J. Geophys. Res.*, *89*, 6847.
- Singhal R. P., and A. Bhardwaj (1991), Monte Carlo simulation of photoelectron energization in parallel electric fields: Electrogrow on Uranus, *J. Geophys. Res.*, *96*, 15963.
- Singhal, R. P., C. H. Jackman, and A. E. S. Green (1980), Spatial aspects of low and medium-energy electron degradation in N₂, *J. Geophys. Res.*, *85*, 1246.
- Spence, D. and G. J. Schulz (1974), Cross section for the production of O₂⁻, and C⁻ by dissociative electron attachment in CO₂: An observation of Renner-Teller effect, *J. Chem. Phys.*, *60*, 216.
- Spielfiedel, A., N. Feautrier, C. Cossart-Magos, G. Chambaud, P. Rosmus, H.-J. Werner, and P. Botschwina (1992), Bent valence excited states of CO₂, *J. Chem. Phys.*, *97*, 8382.
- Spencer L. V., and F. Fano (1954), Energy spectrum resulting from electron slowing down, *Phys. Rev.*, *93*, 1172.
- Straub, H. C., B. G. Lindsay, K. A. Smith, and R. F. Stebbings (1996), Absolute partial cross sections for electron impact ionization of CO₂ from threshold to 1000 eV, *J. Chem. Phys.*, *105* 4015.
- Szmytkowski, C., A. Zecca, G. Karwasz, S. Oss, K. Maciag, B. Marinkovic, R. S. Brusa, and R. Grisenti (1987), Absolute total cross sections for electron-CO₂ scattering at energies from 0.5 to 3000 eV, *J. Phys. B*, *20*, 5817.
- Tanaka, H., T. Ishikawa, T. Masai, T. Sagara, L. Boesten, M. Takekawa, Y. Itikawa, and M. Kimura (1998), Elastic collisions of low to intermediate energy electrons from carbon dioxide: Experimental and theoretical differential cross sections, *Phys. Rev. A*, *57*, 1798.
- Tian, C., and C. R. Vidal (1998), Single to quadruple ionization of CO₂ due to electron impact, *Phys. Rev. A.*, *58*, 3783.
- Tsurubuchi, S., and T. Iwai (1974), Simultaneous ionization and excitation of CO₂ of by electron impact, *J. Phys. Soc. Jpn*, *37*, 1077.
- van der Burgt, P. J. M., W. B. Westerveld, and J. S. Risley (1989), Photoemission cross sections for atomic transitions in the extreme ultraviolet due to electron collisions with atoms and molecules, *J. Phys. Chem. Ref. Data*, *18*, 1757.
- Zecca A., G. Karwasz, and R. S. Bursa (2002), in *Photon and Electron Interaction with Atoms, Molecules and Ions*, edited by Y. Itikawa, Landolt-Börnstein Vol.I/17, Subvolume D (Springer, Berlin).

Table 1. Elastic differential cross section for electron impact on CO₂ (in units of 10⁻¹⁶ cm²/sr)

Energy (eV)	Angle (degree)									
	0	5	10	15	20	30	40	50	60	70
1.5	(1.350) ¹	(1.252)	(1.154)	(1.056)	0.9580	0.7620	0.5410	0.4050	0.3289	0.2957
2.0	(1.157)	(1.055)	(0.954)	(0.852)	0.7505	0.5472	0.3896	0.2455	0.2368	0.2489
3.0	(1.174)	(1.060)	(0.945)	(0.831)	0.7160	0.4868	0.3069	0.3118	0.3386	0.3779
3.8	(2.295)	(2.059)	(1.824)	(1.589)	1.3536	0.8831	0.6294	0.5897	0.5715	0.5367
4.0	(2.007)	(1.844)	(1.681)	(1.517)	1.3536	1.0269	0.7770	0.6857	0.6472	0.5834
5.0	(0.250)	(0.333)	(0.416)	(0.499)	0.5824	0.7486	0.8076	0.8994	0.8079	0.7272
6.0	(0.501)	(0.546)	(0.592)	(0.637)	0.6823	0.7730	0.8244	0.8383	0.8373	0.7644
6.5	(0.933)	(0.914)	(0.896)	(0.878)	0.8599	0.8236	0.9132	0.9286	0.8950	0.6978
7.0	(0.986)	(0.960)	(0.934)	(0.909)	0.8828	0.8313	0.9039	0.9391	0.8025	0.7558
8.0	(16.88)	(12.95)	(9.02)	5.0890	1.1590	1.0020	0.9640	0.8542	0.7214	0.6755
9.0	(24.24)	(18.56)	(12.87)	7.1830	1.4960	1.5880	1.0870	0.9487	0.8375	0.6622
10.0	(39.19)	(29.96)	(20.74)	11.520	2.2977	1.5342	1.2136	0.9926	0.7430	0.6260
15.0	(31.84)	(24.84)	(17.84)	10.843	3.8430	2.7180	1.7789	1.1756	0.7997	0.5777
20.0	(13.80)	(11.77)	(9.743)	7.7149	5.6871	3.2623	1.8542	1.2248	0.7475	0.4324
30.0	(19.89)	(17.10)	(14.31)	(11.52)	8.7310	3.1540	1.4363	0.7430	0.4678	0.3060
40.0	(15.70)	(13.51)	(11.31)	(9.115)	6.9200	2.5300	1.0400	0.5300	0.3100	0.1800
50.0	14.820	12.690	10.560	8.4300	6.3000	2.0400	0.8100	0.4000	0.2100	0.1440
60.0	(13.44)	(11.50)	(9.556)	(7.614)	5.6710	1.7860	0.6597	0.3412	0.1683	0.1109
70.0	(10.61)	(9.055)	(7.50)	(5.945)	4.3900	1.2800	0.5200	0.2500	0.1420	0.1130
80.0	(9.79)	(8.35)	(6.91)	(5.470)	4.0300	1.1500	0.4700	0.2200	0.1360	0.1090
90.0	(8.50)	(7.24)	(5.98)	(4.72)	3.4600	0.9400	0.3800	0.2000	0.1450	0.1120
100.0	(9.273)	(7.893)	(6.514)	(5.134)	3.7543	0.9950	0.3969	0.2026	0.1502	0.1124
200.0	(31.75)	(22.68)	13.610	4.5390	2.4170	0.6160	0.3380	0.2230	0.1270	0.0952
300.0	(19.35)	(13.86)	8.3720	2.8850	1.2350	0.3880	0.2670	0.1290	0.0716	0.0539
400.0	(16.82)	(12.00)	7.1900	2.3770	1.0400	0.4550	0.2150	0.0968	0.0624	0.0523
500.0	(132.80)	77.22	21.600	6.6100	2.7800	1.5600	0.7130	0.3140	0.2190	0.1620
800.0	(138.20)	75.020	11.810	4.1800	2.6500	0.9050	0.3280	0.1900	0.0920	0.0673
1000.0	(113.0)	62.100	11.200	3.5500	2.3500	0.6600	0.2820	0.1430	0.0925	0.0640

Table 1. Contd.

Energy (eV)	Angle (degree)									
	80	90	100	110	120	130	135	150	165	180
1.5	0.2700	0.2405	0.3080	0.3040	0.3567	0.3650	(0.3629)	(0.3816)	(0.3941)	(0.4065)
2.0	0.2765	0.2845	0.3021	0.3276	0.3776	0.3992	(0.4100)	(0.4424)	(0.4748)	(0.5072)
3.0	0.3876	0.3937	0.3950	0.4380	0.4830	0.5173	(0.5345)	(0.5859)	(0.6374)	(0.6888)
3.8	0.5539	0.5739	0.5096	0.5187	0.5280	0.5475	(0.5573)	(0.5865)	(0.6158)	(0.6450)
4.0	0.5595	0.5037	0.4431	0.4217	0.4258	0.4803	(0.5076)	(0.5893)	(0.6711)	(0.7528)
5.0	0.6026	0.4794	0.3910	0.2647	0.2523	0.2853	(0.3018)	(0.3513)	(0.4008)	(0.4503)
6.0	0.6422	0.5258	0.4518	0.3476	0.3136	0.3798	(0.4129)	(0.5122)	(0.6115)	(0.7108)
6.5	0.6616	0.5300	0.4252	0.3390	0.3201	0.3520	(0.3680)	(0.4158)	(0.4637)	(0.5115)
7.0	0.6258	0.5273	0.4333	0.3766	0.3798	0.3724	(0.3687)	(0.3576)	(0.3465)	(0.3354)
8.0	0.6761	0.5343	0.4596	0.4263	0.4058	0.5183	(0.5746)	(0.7433)	(0.9121)	(1.0810)
9.0	0.5799	0.5394	0.4811	0.4381	0.4816	0.6006	(0.6601)	(0.8386)	(1.0170)	(1.1960)
10.0	0.5468	0.4856	0.4478	0.4319	0.5304	0.7077	(0.7964)	(1.0620)	(1.3280)	(1.5940)
15.0	0.4471	0.3596	0.3673	0.4046	0.5445	0.7832	(0.9026)	(1.2610)	(1.6190)	(1.9770)
20.0	0.3516	0.3041	0.3071	0.3887	0.5493	0.6738	(0.7361)	(0.9228)	(1.1100)	(1.2960)
30.0	0.1896	0.1882	0.2391	0.2536	0.3195	0.4441	(0.5064)	(0.6933)	(0.8802)	(1.0670)
40.0	0.1330	0.1190	0.1130	0.1500	0.2400	(0.330)	(0.3750)	(0.5100)	(0.6450)	(0.7800)
50.0	0.1180	0.0920	0.0810	0.1300	0.2500	(0.370)	(0.4300)	(0.6100)	(0.7900)	(0.9700)
60.0	0.0936	0.0911	0.0812	0.01175	0.1805	0.2748	(0.3220)	(0.4634)	(0.6049)	(0.7463)
70.0	0.1040	0.0850	0.0910	0.1400	0.2100	(0.280)	(0.3150)	(0.4200)	(0.5250)	(0.6300)
80.0	0.0900	0.0850	0.0900	0.1200	0.1800	(0.240)	(0.2700)	(0.3600)	(0.4500)	(0.5400)
90.0	0.0804	0.0890	0.0920	0.1200	0.1600	(0.200)	(0.2200)	(0.2800)	(0.3400)	(0.4000)
100.0	0.0840	0.0697	0.0754	0.0880	0.1076	0.1373	(0.1522)	(0.1967)	(0.2413)	(0.2858)
200.0	0.0756	0.0646	0.0709	0.0770	0.0804	0.0878	(0.0944)	(0.1142)	(0.1340)	(0.1538)
300.0	0.0505	0.0376	0.0337	0.0314	0.0272	0.0233	(0.0217)	(0.0169)	(0.0121)	(0.0073)
400.0	0.0376	0.0305	0.0256	0.0255	0.0236	0.0223	(0.0202)	(0.0139)	(0.0076)	(0.0013)
500.0	0.1080	0.0843	0.0752	0.0658	0.0548	(0.0438)	(0.0383)	(0.0218)	(0.0053)	(0.000012)
800.0	0.0523	0.0319	0.0283	0.0238	0.0221	(0.0204)	(0.0195)	(0.0170)	(0.0145)	(0.01190)
1000.0	0.0360	0.0275	0.0220	0.0165	0.0149	(0.0133)	(0.0125)	(0.0101)	(0.0077)	(0.0053)

¹Values inside the bracket indicates a linearly extrapolated value.

Table 2. Parameters for Electron attachment process

	W_P	A	U	W_{th}
O^- -I	4.3	0.0013×10^{-16}	0.22	3.4
O^- -II	8.1	0.0056×10^{-16}	0.33	5.9

Table 3. Parameters for various ionization processes

	W_{th}	I	K	K_B	J	J_B	Γ_S	Γ_B	T_S	T_A	T_B
CO_2^+ (Total)	13.76	13.76	9.83	0.0	40.59	1.050	18.61	-13.23	-0.847	875	44.52
CO_2^+ ($X^2\Pi_g$)	13.76	13.76	3.480	0.0	4.099	-2.35	11.11	-13.26	-0.847	1000	27.52
CO_2^+ ($A^2\Pi_u$)	17.8	17.8	8.632	6.0	86.36	1.004	12.00	-18.80	-1.996	550	10.20
CO_2^+ ($B^2\Sigma_u^+$)	18.1	18.1	4.632	5.0	85.36	1.004	12.00	-18.5	-0.978	450	10.20
CO_2^+ ($C^2\Sigma_g^+$)	19.4	19.4	0.580	0.0	21.19	1.270	10.98	-19.00	-0.887	1000	38.80
CO^+	24.76	24.76	1.347	15.00	6.650	1.256	9.556	-24.0	1.887	800	25.52
O^+	24.5	24.5	2.399	40.00	11.34	-1.10	13.42	-24.0	-0.587	0.0	0.0
C^+	29.5	29.5	1.659	0.0	53.54	0.625	10.62	-29.0	2.800	21.8	44.00
C^{++}	79.94	79.94	0.0012	25.00	0.100	0.656	79.11	0.0	0.8473	0.0	0.0
O^{++}	94	94	0.0055	10.00	1.700	-3.156	20.11	0.0	-0.8473	0.0	0.0
CO_2^{++}	37.6	44.75	0.0583	1.20	0.250	0.0	11.57	35.26	1.548	800	30.52
(CO^+, O^+)	44.7	44.7	0.285	1.200	0.550	0.0	11.97	35.26	1.547	650	30.52
(C^+, O^+)	44.7	44.7	0.288	1.200	0.550	0.0	10.40	45.00	1.547	750	0.0
(O^+, O^+)	44.7	44.7	0.158	1.200	0.450	0.0	5.400	15.00	5.547	750	0.0

Table 4. Parameters for various excitation and emission processes

Excitation states	W	α	β	W_J	Ω	F	$A.F.$
[Vibration, (010)] ¹	0.080	2.750	1.000	0.080	0.750	0.000060	0.0
[Vibration, (100)]	0.180	1.070	1.000	0.180	0.750	0.000031	0.0
[Vibration, (001)]	0.290	2.910	0.500	0.300	0.810	0.000445	0.0
8.6 eV state	8.600	0.556	2.000	8.600	0.936	0.060600	0.0
9.3 eV state	9.300	0.603	2.000	9.300	0.909	0.064000	0.0
11.1 eV state	7.760	0.246	3.000	11.100	1.110	4.420000	0.0
[12.4 eV state]	9.610	0.338	3.000	12.400	0.830	6.700000	0.0
[13.6 eV state]	10.50	0.625	3.000	13.600	0.849	3.350000	0.0
15.5 eV state	15.50	0.739	2.000	15.500	0.793	0.139000	0.750
16.3 eV state	12.30	0.605	3.000	16.300	0.911	0.716000	0.750
17.0 eV state	13.00	0.649	3.000	17.000	0.878	0.114000	0.750
17.8 eV state	14.00	0.977	3.000	17.800	0.725	0.051100	0.750
OI (1304)	20.10	0.599	3.000	22.000	1.000	0.127000	0.750
OI (1356)	16.40	0.600	3.000	20.400	0.944	0.168000	0.500
CI (1279)	15.70	1.000	3.000	26.200	0.643	0.010400	0.500
CI (1329)	21.80	1.000	3.000	20.900	1.040	0.020200	0.500
CI (1561)	22.40	1.000	3.000	24.500	0.982	0.053800	0.500
CI (1657)	21.10	1.000	3.000	24.100	0.947	0.872000	0.500
[CO ⁺ (first negative)]	18.13	0.656	2.54	25.11	0.804	1.055	0.0

¹Parameters are taken from *Jackman et al.* [1977], except for the states which are inside the square brackets whose parameters have been modified.

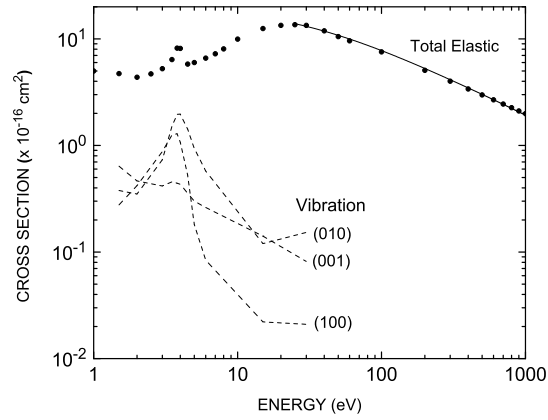


Figure 1. The e-CO₂ total elastic cross section and vibrational excitation cross sections for three modes. For elastic cross section, symbol represents the cross section values of *Itikawa* [2002], and solid curve represents the analytical fit using equation (1). Dashed curve represents the vibrational excitation cross sections taken from *Itikawa* [2002]

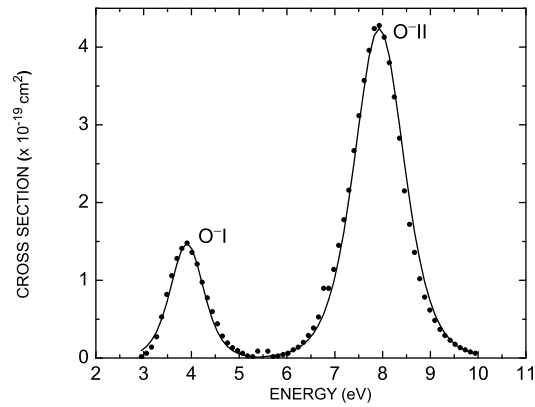


Figure 2. Dissociative electron attachment cross section for the formation of O⁻ ion. Symbol represents the values of *Itikawa* [2002] based on *Rapp and Briglia* [1965]; solid curve represents analytical fit of O⁻ cross section using equation(2). I and II denotes the first and second peak.

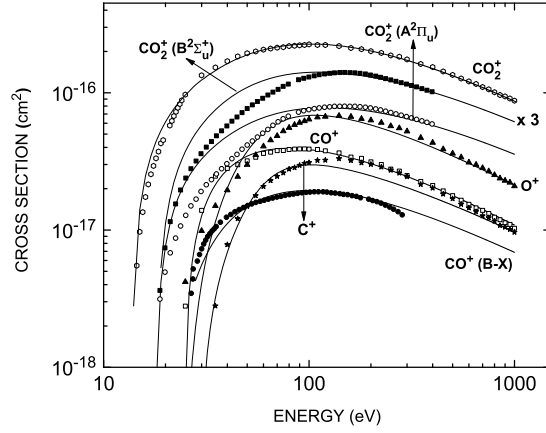


Figure 3. Ionization and emission cross sections of CO_2 . Symbol represents the values of *Itikawa* [2002], and solid curve represents the analytical fits using equation (3) except for $\text{CO}^+(\text{B-X})$ state, which is fitted using equation (4). Note that the cross section for $\text{CO}_2^+(\text{B}^2\Sigma_u^+)$ state has been plotted after multiplying by a factor of 3.

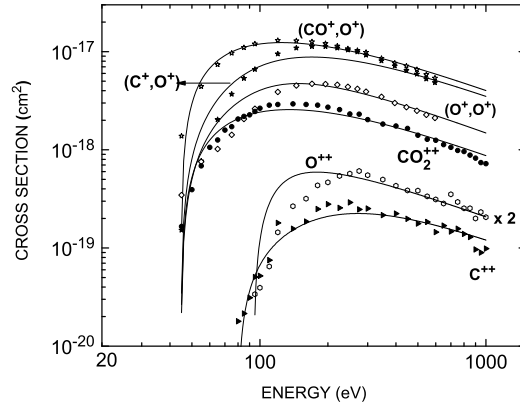


Figure 4. Cross sections for electron impact double ionization of CO_2 . Symbol represents the measured cross section values and solid curve represents the analytical fit using equation (3). Cross sections for $(\text{CO}^+, \text{O}^+)$, (C^+, O^+) , and (O^+, O^+) have been taken from *Tian and Vidal* [1998], and that for CO_2^{2+} , O^{2+} , and C^{2+} from *Itikawa* [2002]. Cross section for O^{2+} has been plotted after multiplying by a factor of 2.

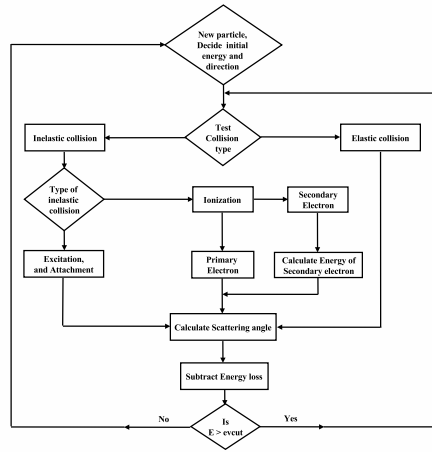


Figure 5. A simplified flow diagram of the Monte Carlo simulation. The diagram shows flow upto secondary electron, but tertiary and subsequent electrons are also treated in a similar manner in the simulation.

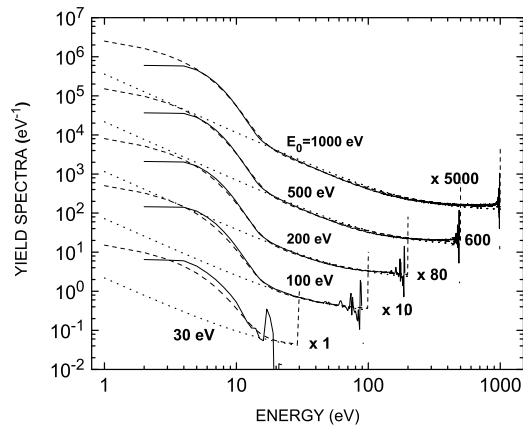


Figure 6. The numerical yield spectra from the Monte Carlo model (solid curve) and AYS using equation (15)(dotted curve) at incident energies (E_0) 30, 100, 200, 500, and 1000 eV. Dashed curve represents the improved AYS calculated by summing equations (15) and (18). The yield spectra at 100, 200, 500, and 1000 eV are plotted after multiplying by a factor of 10, 80, 600, and 5000, respectively.

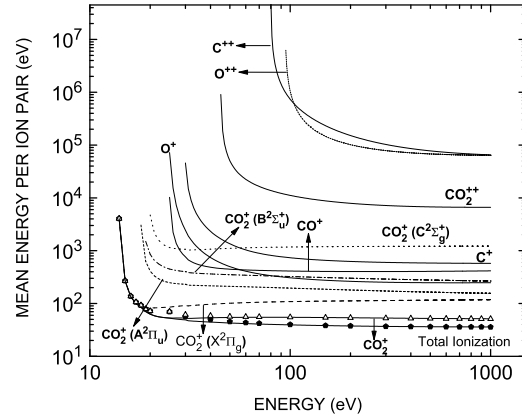


Figure 7. The mean energy per ion pair for ions CO_2^+ (CO_2^+ is the sum of four states $\text{X}^2\Pi_g$, $\text{A}^2\Pi_u$, $\text{B}^2\Sigma_u^+$, and $\text{C}^2\Sigma_g^+$), CO^+ , O^+ , C^+ , CO_2^{++} , O^{++} , and C^{++} , and the neutral CO_2 gas (total), symbol represents the μ calculated using numerical yield spectra for the CO_2^+ and neutral CO_2 .

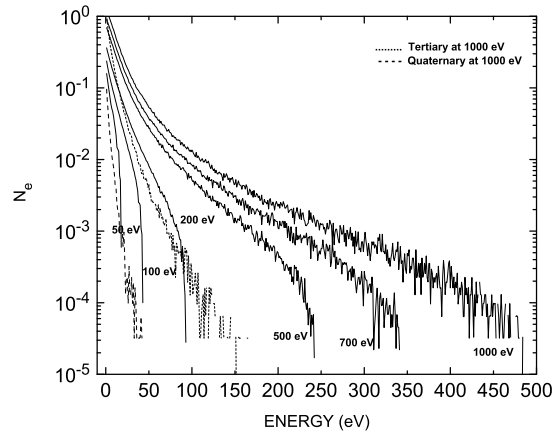


Figure 8. The energy distribution of secondary electrons at six incident energies (E_0): 50, 100, 200, 500, 700, and 1000 eV. N_e represents the number of secondary, tertiary, or quaternary electrons produced per incident primary electron. Dotted curve and dashed curve represent energy distribution of tertiary and quaternary electrons, respectively at $E_0 = 1000$ eV.

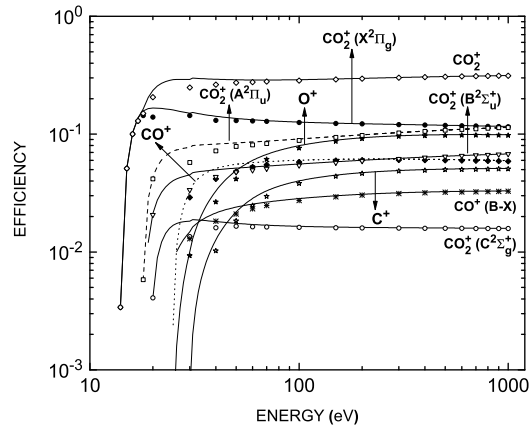


Figure 9. Efficiencies of various ionization and emission processes. Symbol represents the efficiency calculated by numerical yield spectra and curves represent the efficiency calculated by the AYS. $\text{CO}_2^+(\text{A}^2\Pi_u)$ and $\text{CO}_2^+(\text{B}^2\Sigma_u^+)$ represent FDB ($\text{A}^2\Pi_u \rightarrow \text{X}^2\Pi_g$) and ultraviolet doublet ($\text{B}^2\Sigma_u^+ \rightarrow \text{X}^2\Pi_g$) emissions, respectively, and $\text{CO}^+(\text{B-X})$ represents first negative band emission of CO^+ ion.

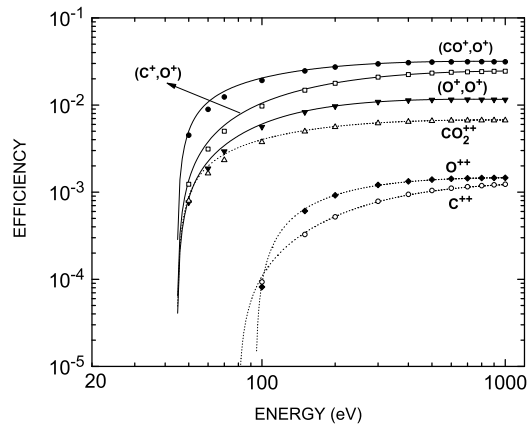


Figure 10. Efficiencies for double ionization of CO_2 due to electron impact. Symbol represents the efficiency calculated by numerical yield spectra and curves represent the efficiency calculated by the AYS.

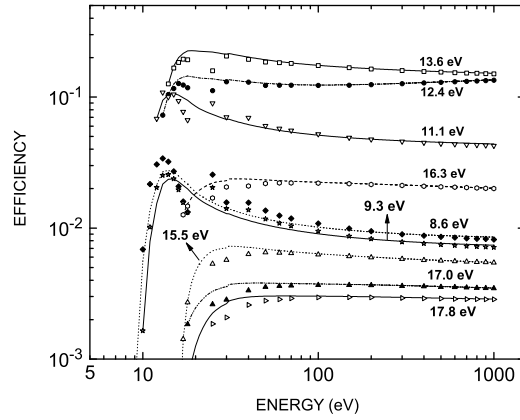


Figure 11. Efficiencies of various excited states. Symbol represents the efficiency calculated by numerical yield spectra and curves represent efficiency calculated by the AYS.

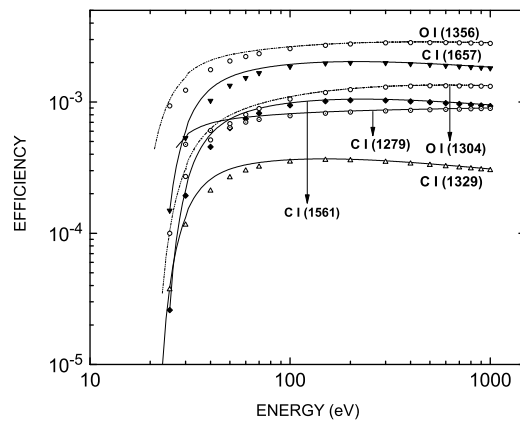


Figure 12. Efficiencies of various oxygen and carbon line emissions. Symbol represents the efficiency calculated by numerical yield spectra and curves represent the efficiency calculated by the AYS.

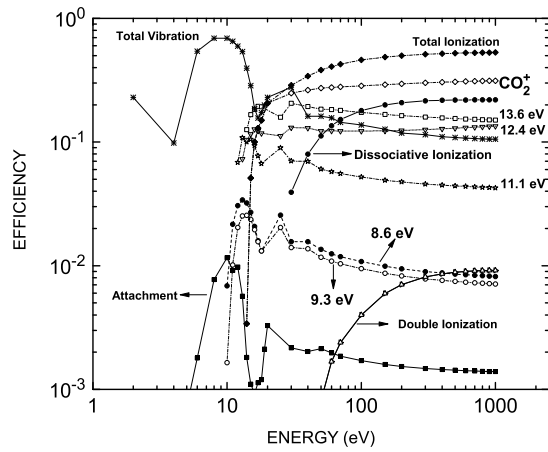


Figure 13. Efficiencies for various important loss channels calculated using numerical yield spectra. Dissociative ionization includes the production of O^+ , C^+ , and CO^+ ions; double ionization includes the production of CO_2^{++} , O^{++} , and C^{++} ions; and attachment denotes the production of O^- ion.